Photobiocatalysis

Light-Controlled Biocatalysis by Unspecific Peroxygenases with Genetically Encoded Photosensitizers

Pascal Püllmann[+], Dominik Homann[+], Tobias A. Karl, Burkhard König, and
Martin J. Weissenborn**

Abstract: Fungal unspecific peroxygenases (UPOs) have gained substantial attention for their versatile oxy-functionalization chemistry paired with impressive catalytic capabilities. A major drawback, however, remains their sensitivity towards their co-substrate hydrogen peroxide, necessitating the use of smart in situ hydrogen peroxide generation methods to enable efficient catalysis setups. Herein, we introduce flavin-containing protein photosensitizers as a new general tool for light-controlled in situ hydrogen peroxide production. By genetically fusing flavin binding fluorescent proteins and UPOs, we have created two virtually self-sufficient photo-enzymes (PhotUPO). Subsequent testing of a versatile substrate panel with the two divergent PhotU-POs revealed two stereoselective conversions. The catalytic performance of the fusion protein was optimized through enzyme and substrate loading variation, enabling up to 24300 turnover numbers (TONs) for the sulfoxidation of methyl phenyl sulfide. The PhotUPO concept was upscaled to a 100 mg substrate preparative scale, enabling the extraction of enantiomerically pure alcohol products.

[*] P. Püllmann,[+] D. Homann,[+] M. J. Weissenborn
Research Group Bioorganic Chemistry, Leibniz Institute for Plant
Biochemistry, Weinberg 3, 06120 Halle (Saale) (Germany)
E-mail: PascalPuellmann@web.de
            martin.weissenborn@chemie.uni-halle.de

D. Homann,[+] M. J. Weissenborn
Institute of Chemistry, Martin-Luther-University Halle-Wittenberg,
Weinbergweg 22, 06120 Halle (Saale) (Germany)

T. A. Karl, B. König
Institute for Organic Chemistry, University of Regensburg, Universitätstr. 31, 93053 Regensburg (Germany)

P. Püllmann[+]
Present address: Molecular Design and Engineering, Bayer AG,
Aprather Weg 18 A, 42113 Wuppertal (Germany)

[+] These authors contributed equally to this work.

Introduction

Nearly 20 years after their initial introduction[1] fungal peroxygenases (UPOs) have established themselves as biocatalysts of high demand within the biocatalysis community[2–4] owing to their versatile oxyfunctionalization chemistry combined with extraordinary reaction stability, enabling impressive turnover numbers (TONs) of up to 300000.[5] One prior bottleneck for the widespread use of UPOs has been their limited accessibility through recombinant standard hosts (yeast and bacteria), thus severely impeding the widespread use and subsequent engineering of this enzyme class. This issue has been addressed in recent years by various research groups, broadening the panel of recombinant UPOs produced in standard hosts, from one enzyme in 2018[6] to approximately 30 in 2023.[7–13]

A second, reoccurring bottleneck is the unique role of hydrogen peroxide in UPO catalysis; while being indispensable for catalysis as a co-substrate, higher concentrations cause oxidative damage, thus impeding high catalytic turnovers. This dilemma has led to the development of a multitude of in situ hydrogen peroxide generating systems for UPO catalysis, ranging from physicochemical to enzymatic supply cascades.[14] Among those systems, the use of visible light as a cheap, readily available energy source for the reduction of O_2 in combination with a diverse catalyst repertoire has been a reoccurring theme.[5,14–19] One of the earliest examples of these systems utilizes flavin mononucleotide (FMN) as a photocatalyst for in situ hydrogen peroxide production.[16]

Flavin and its derivates have been widely used within the field of organic redox photocatalysis in the last decades, enabling a variety of classical redox chemistry, including halogenation and cyanation.[20–22] A protein class that prominently features FMN as an integral component are LOV (light oxygen voltage) proteins.[23] Within this class, bacterial FbFPs (flavin binding fluorescent proteins) have become a popular tool in fluorescent imaging. Contrary to the widespread GFP-based sensors, their maturation does not require oxygen, thus enabling functionality even under hypoxic conditions.[24] In addition to their imaging capabilities, FbFPs have been also increasingly employed for their capabilities as photosensitizers, based on the generation of reactive oxygen species (ROS) such as superoxide, singlet oxygen, and hydrogen peroxide upon reduction of molecular oxygen.[23,25–27] A diverse panel of FbFPs has been characterized regarding the light-dependent killing of *E. coli* through intracellular ROS accumulation, highlighting two

Angew. Chem. Int. Ed. **2023**, *62*, e202307897 (1 of 9)

© 2023 The Authors. Angewandte Chemie International Edition published by Wiley-VCH GmbH

FbFPs as the most potent producers of hydrogen peroxide: EcFbFP (*Bacillus subtilis*) and DsFbFP M49 (*Dinoroseobacter shibae*).[26] In a recent example, FbFP proteins were adapted for in vitro enzyme inactivation, avoiding cross-reactivity within biocatalytic cascade setups by targeted inactivation of a single cascade enzyme post-reaction completion.[28]

In this study, we are utilizing FbFP photosensitizer as a novel concept for the light-induced production of hydrogen peroxide, which as co-substrate for UPO activity, unlocks a versatile panel of oxyfunctionalization chemistry. By using genetically encoded photosensitizers we construct UPO-FbFP fusion proteins performing selective biocatalytic oxyfunctionalizations within a minimal reaction setup. The required supplements are solely buffer, oxygen, and light–thus approaching a concept of self-sufficient UPO catalysis.

Results and Discussion

Design and first testing

The first construction of UPO fusion proteins has recently been reported in an elegant approach.[29] In this study, an evolved UPO was used as the *N*-terminal portion and linked to an evolved aryl alcohol oxidase (AAO). AAOs oxidize aromatic alcohols, producing hydrogen peroxide as a side-product, which then can fuel subsequent UPO chemistry.[29] We used this study as a blueprint regarding the genetic orientation and peptide linker sequences for our study, choosing a subset of four linkers, altering in length and rigidity (Table S1). As photosensitizer candidates, we chose EcFbFP (*Bacillus subtilis*) and the variant DsFbFP M49I (*Dinoroseobacter shibae*) as these have been reported to be the most effective producers of hydrogen peroxide within a panel of commonly employed FbFPs.[26] As UPO targets, we chose two novel long-type UPOs derived from *Psathyrella aberdarensis* (syn. *Candolleomyces aberdarensis*), hereinafter coined as *Pab*UPO I and *Pab*UPO II, which have been reported and characterized in another recent study.[13]

UPO-FbFP (PhotUPO) variant libraries were created by an in-depth shuffling of genetic subunits (signal peptides, UPOs, linkers, and sensitizers) based on previous work on the Golden Gate Assembly-based construction of diversified secretion libraries for UPO.[7,9,30] We chose *Pichia pastoris* (syn. *Komagataella phaffii*) as production host, since previous reports showed beneficial yields of recombinant UPOs relative to *Saccharomyces cerevisiae*.[7,9] Therefore, we constructed a new integrative plasmid (pPAP008), featuring the derepressible/methanol inducible promoter P_{HpFMD} based on the high potential of this promoter to achieve high recombinant UPO yields.[7] The resulting fusion protein libraries were produced in microtiter plates and the supernatant was subsequently screened for UPO activity using the commonly employed DMP assay.[9] After two rounds of rescreening, we could verify two functional fusion proteins in total, namely PabUPO I–Linker C–DsFbFP (hereinafter: PhotUPO-I) and *Pab*UPO II-Linker E- DsFbFP (PhotUPO-II), see Supporting Information for further details. Both

fusion proteins could be obtained in high yield and subsequently purified via His-tag-based affinity purification. The purified samples exhibited a distinct molecular weight pattern, which was slightly reduced after enzymatic deglycosylation with PNGaseF (Figure S2). From the absorption spectra, the presence of both protein components can be clearly deduced for both PhotUPOs, creating a mixed feature with a distinct maximum at 420 nm (UPO heme-thiolate) and two local maxima around 450 and 475 nm (flavin, Figure S2).

The respective single protein components could be successfully produced as well, by using *P. pastoris* (UPOs) and *E. coli*[30] (FbFPs). The obtained SDS gel pattern and absorption spectra of the purified samples (Figure S2) matched the anticipated molecular weight and indicate cofactor incorporation (heme: UPOs and flavin: FbFPs). For all four flavin-containing proteins fluorescence emission spectra) were recorded, being in good agreement with previous reports on FbFPs[23] and indicating no substantial influence of the UPO component (Figure S3).

For initial functional testing, we selected a panel of 17 different sacrificial electron donors (SEDs) as reduction equivalent for flavin in the excited state.[21,31] Focusing on literature known SEDs,[16,31,32] we chose inexpensive and water-soluble additives. As a classical UPO model reaction, the benzylic hydroxylation of ethylbenzene (Figure 1A) was chosen. In the negative control (buffer only), we could not observe any formation of 1-phenyl-1-ethanol, confirming activity being fully dependent on the presence of a suitable SED. Pleasingly, we could identify 11 suitable SEDs, leading to varying degrees of product formation. EDTA (Ethylenediaminetetraacetic acid), glutathione, triethanolamine, and especially ascorbic acid efficiently promoted the hydroxylation reaction. In the special case of using the tertiary amine buffer substances TRIS (tris(hydroxymethyl)aminomethane), HEPES (N-2-hydroxyethylpiperazine-N′-2-ethanesulfonic acid), MES (2-(N-morpholino) ethane sulfonic acid), and MOPS (3-(N-morpholino) propane sulfonic acid), varying product concentrations (Figure 1B) were obtained. This prompted us to switch the default buffer system (100 mM potassium phosphate) to the respective amine buffer compounds.

After succeeding in getting proof of functionality, we set out to investigate the formation of the reaction intermediates superoxide and hydrogen peroxide. Therefore, we added superoxide dismutase (SOD) to accelerate the disproportionation of superoxide to oxygen and hydrogen peroxide. Thus, theoretically supporting UPO performance by facilitating the formation of hydrogen peroxide and minimizing superoxide-caused oxidative damage of the fusion enzyme. Catalase was used as a competitive enzyme for the consumption of hydrogen peroxide, thus theoretically lowering the available amount as PhotUPO co-substrate. Both assumptions could be verified within the experimental setups (Figure 1C). Supplying SOD (orange) accelerated the progression and overall amount (+58 %) of the alcohol product in comparison to the reaction control without accessory enzyme addition (red). The addition of catalase (1000 units; green) suppressed UPO activity effi-
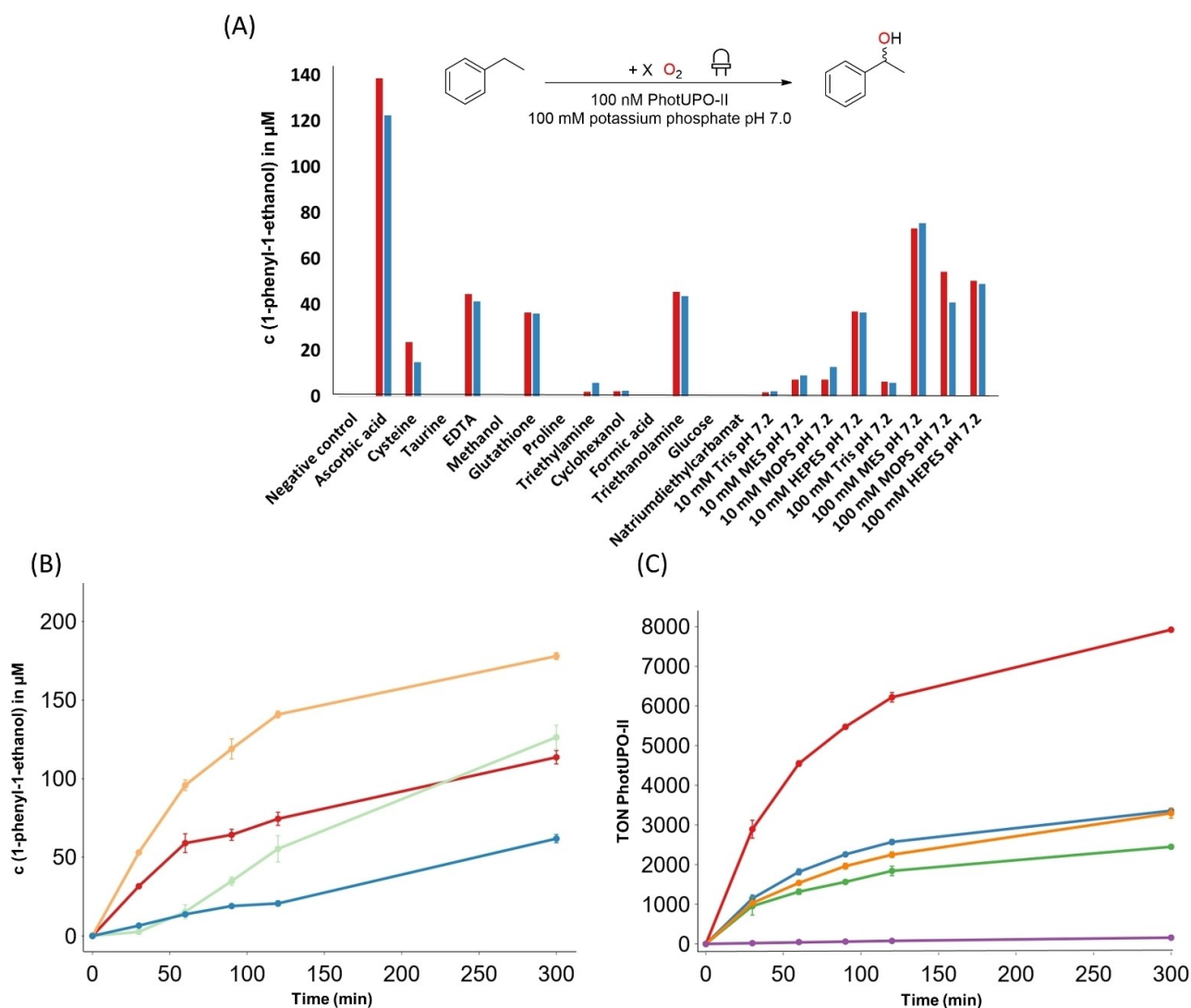
Figure 1. Functionality testing of the PhotUPO concept. A) PhotUPO activity was investigated through GC-MS analysis of the benzylic hydroxylation of ethylbenzene. Set of 17 electron donors (labeled X) was chosen and added (10 mM) to the reaction. Alterations are labeled in the chart, as in case of 100 mM MES, MOPS, HEPES and Tris the default buffer system (100 mM potassium phosphate 7.0) was omitted. Reactions performed as independent duplicates for 1 h and 0.4 W/slot blue light. B) Investigating the role of reaction intermediates. 8 mL reaction setups (100 mM HEPES pH 7.2, 100 nM PhotUPO-II, 5 mM ethylbenzene, 5% v/v acetone, 0.8 W/slot blue light) were run for 300 min; 1 mL samples were taken after 30, 60, 90, 120 and 300 min and analyzed by GC-MS. Red: without addition; orange: addition of 450 units superoxide dismutase (from start); green: addition of 1000 units catalase (from start) and blue: addition of 200 units catalase (from start) and 100 units after 30, 60, 90, 120 min (in total: 700 units). Data points derived from three independent reactions and standard deviations indicated as error bars. C) Comparison of different setups for photo-based UPO catalysis. Total turnover of UPO activity as in (A) and (B). 7.25 mL reaction setups (100 mM HEPES pH 7.2, 5 mM ethylbenzene, 5% v/v acetone, 0.8 W/slot blue light) were run for 300 min; 1 mL samples were taken after 30, 60, 90, 120 and 300 min and analyzed by GC-MS. Violet: 100 nM *Pab*UPO II; green: 100 nM FMN and 100 nM *Pab*UPO II; orange: 100 nM EcFbFP and 100 nM *Pab*UPO II; blue: 100 nM PhotUPO-II and red: 100 nM DsFbFP and 100 nM *Pab*UPO II. Data points collected from three independent measurements and the standard deviations indicated as error bars.

ciently within the first interval (approx. 8% product amount of positive control) but led to slightly higher overall product formation after the total reaction time, indicating instability of catalase over the reaction period (Figure 1C). This could be verified when starting the reactions with 200 units (blue) and adding 100 units respectively at every measurement point, yielding a total amount of 700 units. A nearly linear product formation could be observed, leading to approx.

53% of the total product amount compared to the control (red).

As final aspect of the initial characterization, we verified the necessity for both fusion components for activity and investigated their respective stability. We could observe just a minimal product formation when using *Pab*UPO II (purple) without the addition of any photocatalyst compared to the PhotUPO-II reaction (blue; Figure 1D). This observation can be explained by small amounts of hydrogen

peroxide formed in HEPES buffer upon irradiation, as reported previously.[33] To benchmark the efficiency of our fusion system (blue), we included a state-of-the-art flavin mononucleotide (FMN) system for hydrogen peroxide production (green) as comparison.[16] The 37 % increased catalytic performance of the PhotUPO system in comparison to FMN in combination with PabUPO II (3358 vs. 2449 TON), indicates a beneficial performance of the protein-associated flavin photocatalyst. This effect is even more pronounced when using DsFbFP and PabUPO II as single components (red). In this case, the highest final TON values of 7921 were obtained, outperforming the system with free FMN (+223 %) as well as the respective fusion of both components (PhotUPO-II; +135 %). When using EcFbFP and PabUPO II (orange), this trend could not be verified as comparable TON values (3295 TON) to PhotUPO-II were obtained. This indicates inferior stability of the EcFbFP sensitizer, which also might relate to the fact that both identified PhotUPOs contain DsFbFP as a photosensitizer unit.

Comparing different illumination strengths (Figure S4), we could not observe a clear tendency towards a defined value but reached the best catalytic performance at 0.4 as well as 0.8 W/slot illumination strength. Subsequent reactions were performed using either 0.8 or 1.0 W/slot illumination strength as default values, ensuring the best performance.

We then focused on investigating the stability of the system components, as prior results (Figures 1 C and 1D) indicated a decreasing enzyme activity over reaction time. Using PhotUPO-II as a catalyst within a 300 min reaction interval, the first 120 min contributed to approx. 80 % of product formation (Figures 1 C and 1D). To enable continuous observation, we switched the assay from a discontinuous GC-MS assay to a spectroscopic assay. The oxidation of veratryl alcohol was chosen as common UPO assay,[1] since product formation can be conveniently monitored at $\lambda = 310$ nm.

We first investigated different excitation wavelengths (451 or 471 nm; Figure S6). 451 nm proved to be the superior, enabling longer stability preservation and a higher product formation (+8 %). Thus, all subsequent measurements were conducted at this wavelength. Comparing the reaction stability of PhotUPO-I and PhotUPO-II, substantial differences could be observed (Figure S7). PhotUPO-I proved to be highly active within the measurement interval, sustaining a linear reaction velocity for approximately 90 min (30 to 140 min). The activity of PhotUPO-II, in contrast, rapidly declined after sustaining a linear reaction velocity for approx. 50 min (20 to 70 min), matching prior observations regarding the sharp decrease of activity after 120 min (Figures 1 C and 1D).

Based on the observations that using DsFbFP and PabUPO II as individual components in comparison to their respective fusion, PhotUPO-II led to a more than doubled product formation (Figure 1D) we revisited this setup (Figure 2B). The single components (red) enabled a nearly perfect linear reaction progression, which could even be prolonged to a 6 h reaction time (Figure S8)– indicating

extraordinary stability of both single protein components in the photocatalytic setup. PhotUPO-II exhibited a lag time of approximately 20 min before reaching linear reaction velocity (similarly observed for PhotUPO-I). The obtained linear reaction velocity of the fusion protein is substantially higher, therefore also resulting in higher momentarily product concentrations for the majority of the measurement interval (23 min to 133 min). However, as observed before, rapid inactivation occurred after approx. 70 min.

Choosing the more stable fusion protein PhotUPO-I we set out to test the external control of the fusion system by light. One major advantage of using a light-driven system is the facile control of activity (on/off) by applying illumination or darkness conditions accordingly (Figure 2C). While observing no substantial product formation in darkness (green), the illuminated samples exhibited the expected switch pattern. After illumination for 1 h (red), product formation first decreased and completely stopped after switching the sample to dark conditions (another 2 h). Following the switching, the sample showed a slow decrease of activity over 30 min, which is most likely based a continued consumption of residual hydrogen peroxide by the UPO portion. Hence, no sharp on/off transition could be obtained, indicating that the fusion proteins rather exhibit pronounced on- and off-lag phases of activity ranging around 20 to 30 min (see also Figs. S7 and 2B). Analogous measurements were also performed for PhotUPO-II (Figure S9).

To deconvolute the instable components within the PhotUPO-II fusion system (Figure 2B) we investigated this aspect by spiking different protein components. All reactions were started using 40 nM of PhotUPO-II and run for 180 min (Figure 2D). When adding no further components (red), the reaction rate substantially decreased within the last 60 min. A similar behavior could be observed when adding 40 nM DsFbFP (orange) after 120 min, strongly implying the UPO to be the unstable portion, as the addition of new photocatalyst could not increase UPO product formation further. This hypothesis was validated when adding 40 nM PabUPO II (blue), which led to a strong linear increase of product formation, suggesting the photocatalyst portion (DsFbFP) still being functional and supplying hydrogen peroxide to be converted by the freshly added UPO. A final reaction (green), adding 40 nM of PabUPO II and 40 nM DsFbFP, revealed a similar pattern of strong linear product increase within the last 60 min. Taking this observation and the impressive stability of the single components (Figure S8) into account – it can be deduced that the freely diffusing UPO is highly stable under the chosen reaction conditions, but that the PhotUPO fusion conditions, such as linker length and rigidity, as well as potentially enhanced local oxidative damage through the occurrence of ROS, lead to an accelerated UPO deactivation. This deduction offers a starting point for subsequent directed evolution endeavors to increase the UPO stability and consequently the catalytic performance of the PhotUPO fusion.
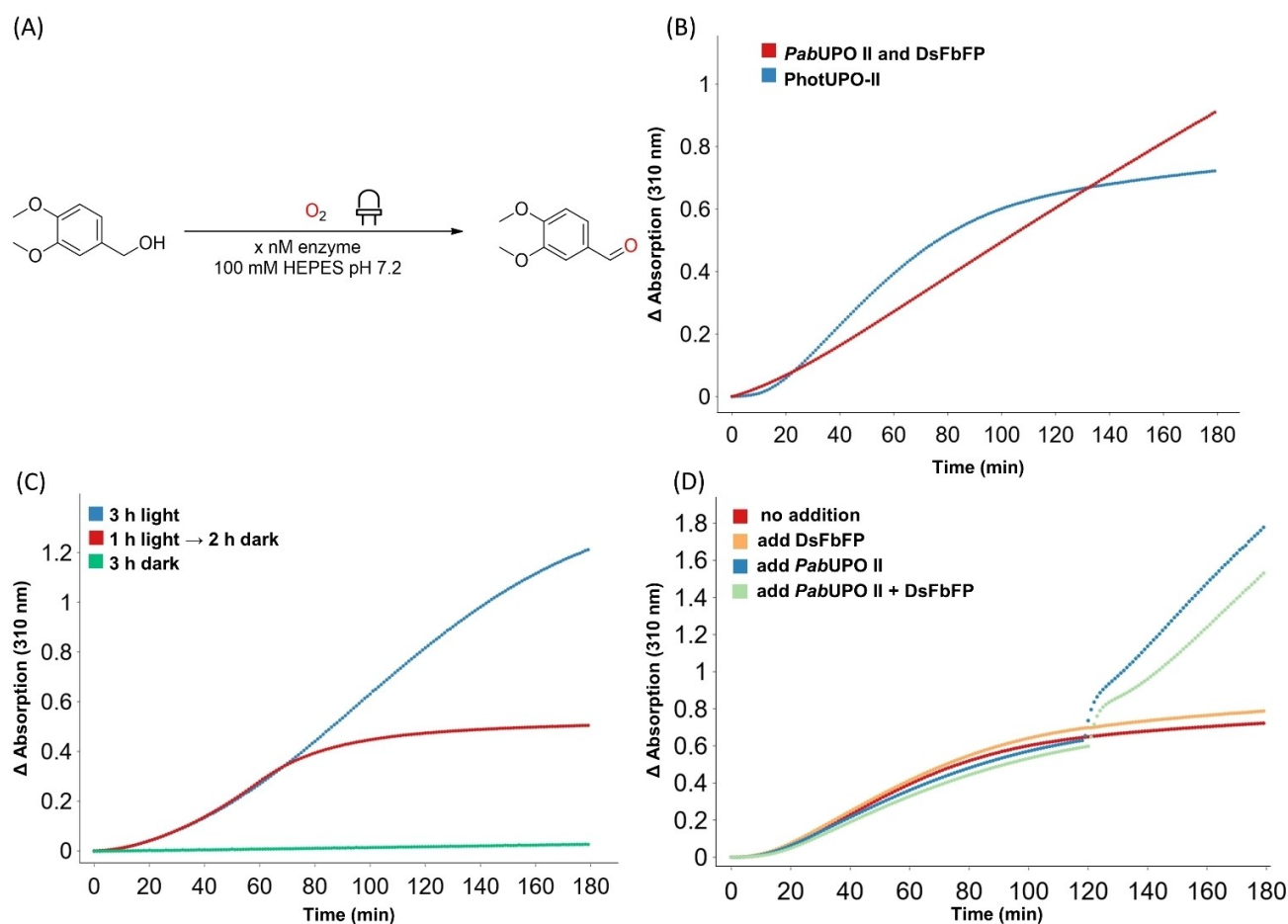
Figure 2. Continuous PhotUPO measurements for stability assessment. A) Continuous measurements performed by employing oxidation of veratryl alcohol as reference reaction (λ=310 nm). Data points obtained within a 60 s interval. Reaction mixtures consisted of 100 mM HEPES pH 7.2 and 10 mM veratryl alcohol. Samples were illuminated by a LED spot (1 W and 451 nm; Figure S5). B) Comparison of the catalytic performance of the fusion protein (PhotUPO-II; blue) and the respective single component proteins DsFbFP and *Pab*UPO II (red), utilizing 40 nM. C) Switch measurements of PhotUPO-I (40 nM). Measurements conducted under 3 h illumination (blue), 1 h initial illumination and 2 h of subsequent darkness (red) and 3 h darkness (green). D) Deconvolution of the activity. All reactions were started with 40 nM PhotUPO-II and run similar for the first 120 min. The control (red) was continued for another 60 min. In case of the other reactions protein combinations were quickly added at t=120 min. These are 40 nM DsFbFP (orange), 40 nM *Pab*UPO II (blue) and the addition of 40 nM *Pab*UPO II and 40 nm DsFbFP (green).

Optimization of the catalytic performance

After evaluating the functionality (Figure 1) and delineating the performance (Figure 2), we performed further optimization reactions regarding physical/chemical parameters to further boost the catalytic performance. Increasing the available amount of molecular oxygen did not yield a positive effect (Figure S10). pH effects were investigated using either 100 mM MES or HEPES buffers in a pH range of 5.5 to 7.2, as both had previously been identified as suitable donor/buffer systems (Figure 1A). Within our fusion- and ethylbenzene reaction setups (SI Figures 11 and 12), we identified optimal pH values for PhotUPO-I (pH 6.5) and PhotUPO-II (pH 7.2). As a final aspect, we identified a substantial enhancement by the addition of ascorbic acid (10 mM) as an extra electron donor for the PhotUPO-I (+32%) and PhotUPO-II (+195%) constructs (Figure S13).

Investigation of substrate preference

We next examined the chemical activity and selectivity of both PhotUPOs towards a versatile panel of substrates (Figure 3). Therefore, we studied a subset of four benzylic hydroxylation, one epoxidation and two sulfoxidation reactions. Ethylbenzene was efficiently converted to the benzylic alcohol by both fusions (Figure 3), albeit with a lower selectivity (PhotUPO-I: 84% *ee (R)* and PhotUPO-II: 90% *ee (R)*) as the well-characterized UPO from *Agrocybe aegerita* (*Aae*UPO), exhibiting ≥99% selectivity for the formation of the *R*-enantiomer.[16,34] Utilizing propylbenzene, the reaction behavior of both enzymes proved to be highly divergent. While PhotUPO-I barely converted propylbenzene, PhotUPO-II (1025 TON) yielded an excellent stereoselectivity of >99% *(R)*, almost identical to the absolute stereoselectivity observed for *Aae*UPO.[34] Benzylic hydroxylation of butylbenzene proved inefficient, as both enzymes
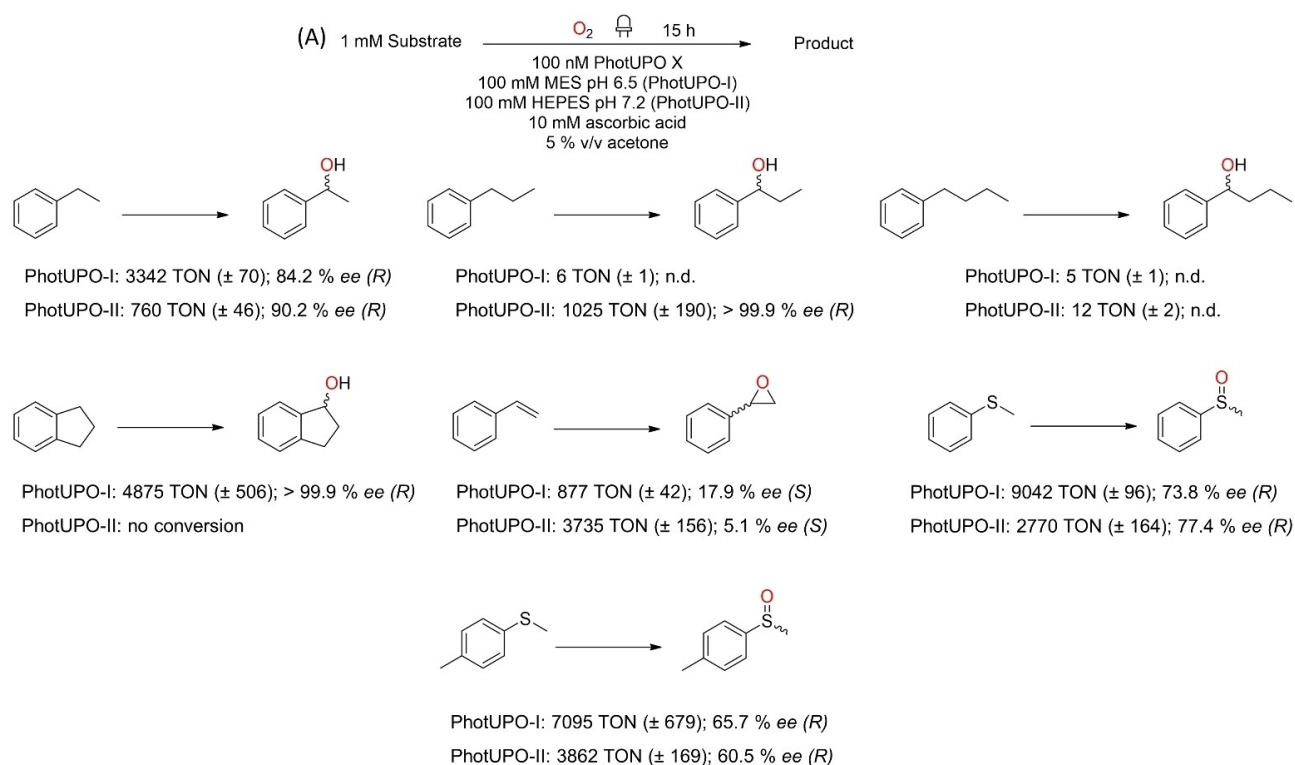
Figure 3. Screening of a diverse UPO substrate panel for conversion by PhotUPO-I and PhotUPO-II. A) Reactions performed as three independent measurements (n = 3) following the reaction details given at an illumination strength of 0.8 W/slot. TONs determined by achiral GC-MS analysis and normalization to calibration curves (Figure S14). Standard deviations are given as ± values. Samples analyzed via chiral GC-MS to determine the enantiomeric excess (ee) and determine the enantiomers through comparison with authentic product standards. Within all chiral measurement setups all standard deviations are ≤ 6 %. Enantiomeric distributions and their comparison to racemic or single standards are summarized in Figure S15. n.d. = not determined.

preferentially catalyzed the formation of various hydroxylation products at the 2 and 3 positions (Figure S16).

The conversion of indane by PhotUPO-I (4875 TON) yielded excellent stereoselectivity (> 99 %; Figure S15) for the formation of 1-(R)-indanol, therefore adding another stereoselective conversion to the current UPO reaction portfolio. UPO-catalyzed indane conversion using *Aae*UPO (87 % ee (R))[34] and the L60F variant of *Mth*UPO (95 % ee (R))[10] did not achieve absolute stereoselectivity.

The epoxidation of styrene could be efficiently catalyzed by both PhotUPOs (Figure 3), yielding 877 (PhotUPO-I) and 3735 (PhotUPO-II) TON respectively. The overall low enantiomeric excess of the (S)-epoxide enantiomer of 18 % ee (PhotUPO-I) and 5 % ee (PhotUPO-II) aligns well with a previously reported general low preference for the (S)-enantiomer in the case of *Aae*UPO (2 % ee), *Tte*UPO (4 % ee), *Mro*UPO (30 % ee), *Cgl*UPO (44 % ee) and the currently most selective UPO *Mth*UPO (45 % ee).[9]

As final reaction type, we investigated the sulfoxidation of methyl phenyl sulfide and methyl p-tolyl sulfide. Both substrates were efficiently converted leading to enantiomeric excesses of the respective (R)-enantiomers in the range of 61 to 77 % ee. Especially PhotUPO-I proved to be an efficient catalyst for sulfoxidation, leading to complete (methyl phenyl sulfide) and nearly complete substrate conversion (methyl p-tolyl sulfide). Analogously to Bier-

baumer et al.,[35] we observed a substantial background sulfoxidation reaction when performing the photocatalytic reactions without catalyst addition, which was considered in the final TON values. Due to the background reaction being non-selective, the ee values of PhotUPO reactions were negatively affected.

We set out to further increase the catalytic performance by examining variations in enzyme and substrate load. We chose the hydroxylation of propylbenzene (PhotUPO-II) due to its high selectivity and the sulfoxidation of methyl phenyl sulfide (PhotUPO-I) with quantitative substrate conversion. Substrate loadings were increased to 3.5 mM (propylbenzene) and 5 mM (methyl phenyl sulfide; Figure S17). The propylbenzene setup led to an almost doubled TON (1023 to 1925) when using same enzyme loading (100 nM) as before (Figure 3). By increasing the loading to 600 nM the performance was further increased to 5258 TON, presenting a 5.1-fold improvement and obtaining a 90 % analytical yield of 1-phenyl-1-propanol. The comparison of a similar reaction setup with the single components DsFbFP and *Pab*UPO II (100 nM each) did not lead to any product (Figure S18). There seems to be a not generalizable beneficial effect of using photosensitizer and UPO as single protein components, necessitating further investigations on the reaction behavior of both systems.

The sulfoxidation of methyl phenyl sulfide by PhotUPO-I already led to full conversion under low catalyst loading (100 nM; Figure 3). When investigating higher loadings, we again observed a substantial background reaction in the absence of catalyst (Figure S17). Contrary to the hydroxylation of propylbenzene by PhotUPO-II, an increased enzyme load did not increase catalytic performance. Optimal catalytic performance was achieved at 100 nM amounting to a 2.7-fold increased TON of 24323 TON. 200 nM loading proved sufficient to achieve nearly full conversion (95%) of 5 mM sulfide substrate.

Upscaling of the concept to a preparative scale

To illustrate the applicability of the presented work, three reactions were realized in a preparatively useful scale. We chose the benzylic hydroxylation of propylbenzene (PhotUPO-II), the benzylic hydroxylation of indane (PhotUPO-I), and the sulfoxidation of methyl phenyl sulfide (PhotUPO-I).

For this purpose, the setup was upscaled from a photo-reactor (max. 8 mL) to a round-bottom flask setup (approx. 200 mL), which was illuminated with a commercial LED strip (Figure S20). Due to the higher required protein amounts, protein purification was omitted, and instead the concentrated (approx. 20-fold) and sterile filtered (0.2 µM) supernatant from *P. pastoris* was used. Enzyme concentration was adjusted to 1 µM and substrate loadings were adjusted to 5 mM (indane and propylbenzene) and 15 mM (methyl phenyl sulfide). To enable complete solubilization of the substrates, the amount of co-solvent (acetone) was increased to 10% v/v. The reactions were carried out at room temperature under constant magnetic stirring, with a substrate amount of 100 mg.

We obtained nearly full (indane) and full conversions (propylbenzene and methyl phenyl sulfide; Figure 4). In this setup the occurrence of the overoxidation products indanone, 1-phenyl-1-propanone as well as methyl phenyl sulfone, respectively, became notable. This observation was especially pronounced for the hydroxylation of propylben-
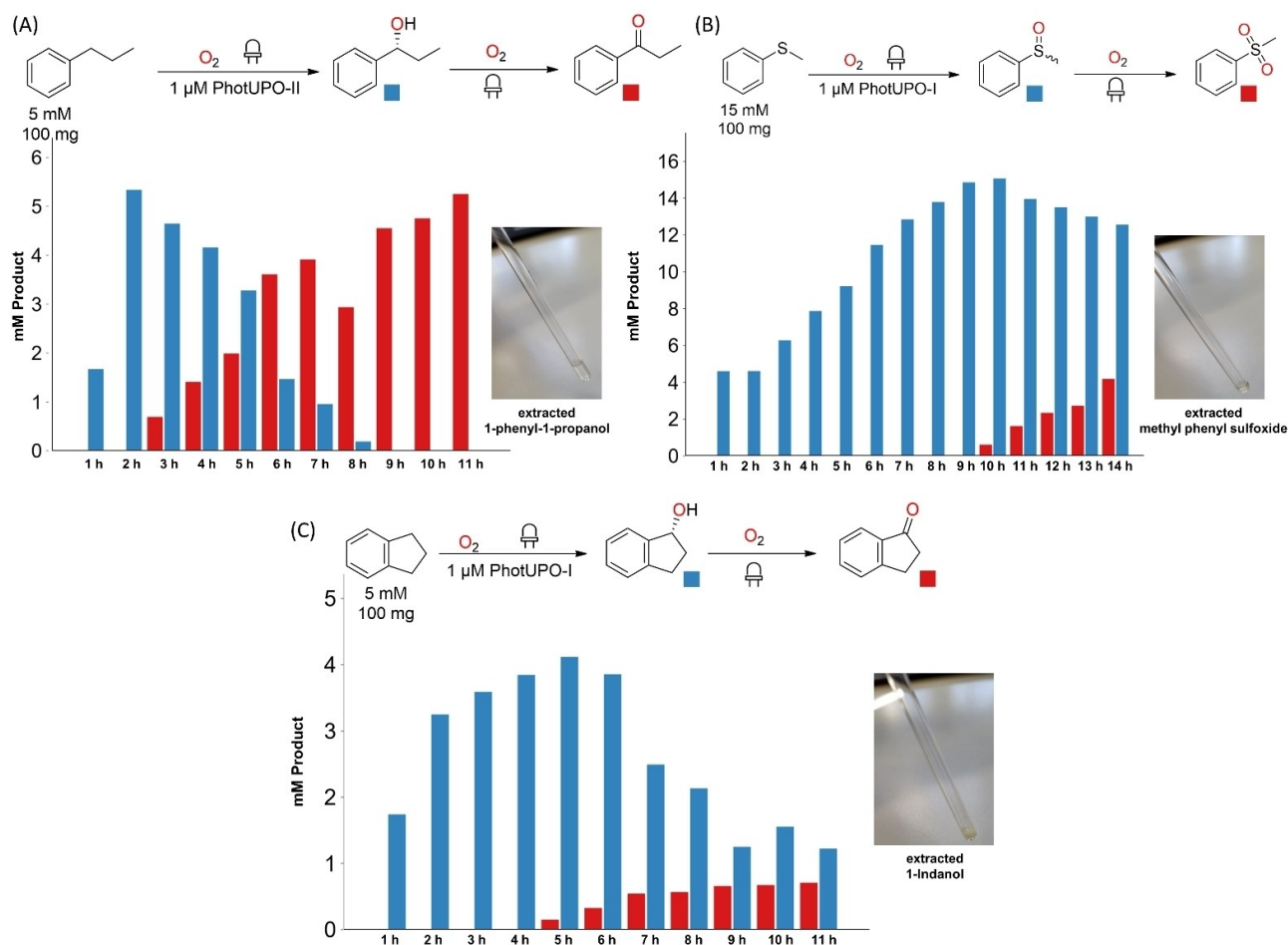

Figure 4. Upscaling of the PhotUPO concept to a preparative scale. Upscaling reactions performed in round bottom flasks illuminated by a standard commercial LED strip (44 W, 3 m; setup: Figure S20. Samples taken after indicated time points and analyzed by GC-MS for the two analytes (blue and red) as indicated Adjusted calibration curves were used for product quantification (Figure S19). Respective first-stage oxidation products of the reactions were extracted, purified and verified by ^{1}H NMR spectroscopy (see SI; section V- NMR Spectra). Chiral separation of the products and *ee* values are displayed in Figure S22. Exemplary time course progressions of the respective reactions, from an analogous measurement setup are displayed in Figure S21.

zene by PhotUPO-II (Figure 4A). The substrate was completely converted to 1-phenyl-1-propanol after 120 min and subsequently completely oxidized to 1-phenyl-1-propanone after 11 h. Using 1 µM PhotUPO and 5 mM substrate loading, 10000 TON could be achieved, thus clearly outperforming even the optimized analytical yields (5258 TON) from before (Figure S17). Less pronounced overoxidation for methyl phenyl sulfide (Figure 4B) and indane (Figure 4C), lead to a proportion of 17 % (indanone) and 28 % (methyl phenyl sulfone) of the overall maximal product yield of the first reaction product. Based on the enzyme and substrate loading, overall catalytic efficiencies of approx. 19000 TON for the sulfoxidation (Figure 4B) and approx. 5000 TON for indane conversion (Figure 4C) were obtained. Time course progressions of substrate depletion as well as the formation of the first and second reaction products, derived from a second comparable reaction setup, are displayed in Figure S21.

Remarkably, the stability of the PhotUPO fusions in the preparative experimental setups appears to be superior despite the increase of the co-solvent fraction to 10 % v/v, allowing constant conversion for 11 (indane, propylbenzene) to 14 h (methyl phenyl sulfide) without apparent enzyme deactivation. This observation is in sharp contrast to the pronounced enzyme deactivation previously observed on an analytical scale, which occurred after a reaction time of only 2–3 h (Figures 1 C, 2B, and 2 C). Thus, the occurrence of subsequent overoxidation can most likely be linked to the prolonged reaction time of the UPO.

Conclusion

We introduce flavin-binding fluorescent proteins (FbFPs) as a new concept for fueling hydrogen peroxide-dependent biocatalysis, enabling the spatial tunable control of enzyme activity by light. Initial characterization experiments revealed that FbFPs are powerful protein-based photosensitizers, allowing a more than 2-fold increase in catalytic UPO turnover compared to free FMN. We envision that the FbFP-fusion concept will be broadly applicable to fuel other hydrogen peroxide-consuming enzymes such as peroxidases, oxidases, and P450 enzymes. Being protein-based and therefore genetically encoded, FbFPs are furthermore amendable to optimization by applying directed evolution to enhance stability, selectivity for specific wavelengths, and efficiency amongst other factors. Directed evolution can be expanded toward the complete coding sequence. As the UPO portion proved to be the less stable component an additional emphasis can be placed on the length and constitution of the linker connecting both proteins. The first report of engineering photo-enzymes in a high-throughput 96 well plate system has been recently reported.[36]

We proved that the PhotUPO fusion setup performs under minimal reaction requirements, simply necessitating buffer (electron source), oxygen, and light (reduction power)– approaching a concept of self-sufficient UPO catalysis. This further simplifies previously reported photosensitizer systems,[37] which depended on the external feeding of chemical sensitizers and using the generated electron flow for reductions in vivo.

We believe that the PhotUPO concept can open new avenues in photo-biocatalysis. By being fully genetically encoded as well as continuously secreted by *P. pastoris*, the implementation of PhotUPOs into continuous flow-photocatalysis setups[38] is an obvious perspective. On a broader scope, it would be extremely valuable to combine PhotUPO biocatalysis with classical organic photoredox catalysis in the future, harnessing the high potential of both disciplines.

Conflict of Interest

The authors declare no conflict of interest.

Data Availability Statement

The data that support the findings of this study are available in the supplementary material of this article.

[1] R. Ullrich, J. Nüske, K. Scheibner, J. Spantzel, M. Hofrichter, *Appl. Environ. Microbiol.* **2004**, *70*, 4575–4581.

[2] M. Hobisch, D. Holtmann, P. Gomez de Santos, M. Alcalde, F. Hollmann, S. Kara, *Biotechnol. Adv.* **2021**, *51*, 107615.

[3] D. T. Monterrey, A. Ménes-Rubio, M. Keser, D. Gonzalez-Perez, M. Alcalde, *Curr. Opin. Green Sustain. Chem.* **2023**, *41*, 100786.

[4] J. Münch, P. Püllmann, W. Zhang, M. J. Weissenborn, *ACS Catal.* **2021**, *11*, 9168–9203.

[5] W. Zhang, E. Fernández-Fueyo, Y. Ni, M. Van Schie, J. Gacs, R. Renirie, R. Wever, F. G. Mutti, D. Rother, M. Alcalde, F. Hollmann, *Nat. Catal.* **2018**, *1*, 55–62.

[6] P. Molina-Espeja, E. Garcia-Ruiz, D. Gonzalez-Perez, R. Ullrich, M. Hofrichter, M. Alcalde, *Appl. Environ. Microbiol.* **2014**, *80*, 3496–3507.

[7] P. Püllmann, M. J. Weissenborn, *ACS Synth. Biol.* **2021**, *10*, 1360–1372.

[8] A. Knorrscheidt, P. Püllmann, E. Schell, D. Homann, E. Freier, M. J. Weissenborn, *ChemCatChem* **2020**, *12*, 4788–4795.

[9] P. Püllmann, A. Knorrscheidt, J. Münch, P. R. Palme, W. Hoehenwarter, S. Marillonnet, M. Alcalde, B. Westermann, M. J. Weissenborn, *Commun. Biol.* **2021**, *4*, 562.

[10] A. Knorrscheidt, J. Soler, N. Hünecke, P. Püllmann, M. Garcia-Borràs, M. J. Weissenborn, *ACS Catal.* **2021**, *11*, 7327–7338.

[11] K. Ebner, L. J. Pfeifenberger, C. Rinnofner, V. Schusterbauer, A. Glieder, M. Winkler, *Catalysts* **2023**, *13*, 206.

[12] A. Kinner, K. Rosenthal, S. Lütz, *Front. Bioeng. Biotechnol.* **2021**, *9*, 705630.

[13] P. G. de Santos, M. D. Hoang, J. Kiebist, H. Kellner, R. Ullrich, K. Scheibner, M. Hofrichter, C. Liers, M. Alcalde, *Appl. Environ. Microbiol.* **2021**, *87*, e00878–21.

[14] B. O. Burek, S. Bormann, F. Hollmann, J. Z. Bloh, D. Holtmann, *Green Chem.* **2019**, *21*, 3232–3249.

[15] C. H. Yun, J. Kim, F. Hollmann, C. B. Park, *Chem. Sci.* **2022**, *13*, 12260–12279.

[16] E. Churakova, M. Kluge, R. Ullrich, I. Arends, M. Hofrichter, F. Hollmann, *Angew. Chem. Int. Ed.* **2011**, *50*, 10716–10719.

[17] B. Yuan, D. Mahor, Q. Fei, R. Wever, M. Alcalde, W. Zhang, F. Hollmann, *ACS Catal.* **2020**, *10*, 8277–8284.

[18] S. J. P. Willot, E. Fernández-Fueyo, F. Tieves, M. Pesic, M. Alcalde, I. W. C. E. Arends, C. B. Park, F. Hollmann, *ACS Catal.* **2019**, *9*, 890–894.

[19] M. M. C. H. Van Schie, W. Zhang, F. Tieves, D. S. Choi, C. B. Park, B. O. Burek, J. Z. Bloh, I. W. C. E. Arends, C. E. Paul, M. Alcalde, F. Hollmann, *ACS Catal.* **2019**, *9*, 7409–7417.

[20] T. Hering, B. Mühldorf, R. Wolf, B. König, *Angew. Chem. Int. Ed.* **2016**, *55*, 5342–5345.

[21] B. König, S. Kümmel, E. Svobodová, R. Cibulka, *Phys. Sci. Rev.* **2019**, *3*, 20170168.

[22] N. P. Ramirez, B. König, J. C. Gonzalez-Gomez, *Org. Lett.* **2019**, *21*, 1368–1373.

[23] M. Wingen, J. Potzkei, S. Endres, G. Casini, C. Rupprecht, C. Fahlke, U. Krauss, K. E. Jaeger, T. Drepper, T. Gensch, *Photochem. Photobiol. Sci.* **2014**, *13*, 875–883.

[24] T. Drepper, T. Eggert, F. Circolone, A. Heck, U. Krauß, J. K. Guterl, M. Wendorff, A. Losi, W. Gärtner, K. E. Jaeger, *Nat. Biotechnol.* **2007**, *25*, 443–445.

[25] S. Endres, J. Granzin, F. Circolone, A. Stadler, U. Krauss, T. Drepper, V. Svensson, E. Knieps-Grünhagen, A. Wirtz, A. Cousin, P. Tielen, D. Willbold, K. E. Jaeger, R. Batra-Safferling, *BMC Microbiol.* **2015**, *15*, 30.

[26] S. Endres, M. Wingen, J. Torra, R. Ruiz-González, T. Polen, G. Bosio, N. L. Bitzenhofer, F. Hilgers, T. Gensch, S. Nonell, K. E. Jaeger, T. Drepper, *Sci. Rep.* **2018**, *8*, 15021.

[27] T. Fettweiss, K. Röllen, J. Granzin, O. Reiners, S. Endres, T. Drepper, D. Willbold, K. E. Jaeger, R. Batra-Safferling, U. Krauss, *Biochemistry* **2018**, *57*, 4833–4847.

[28] T. Gerlach, J. Schain, S. Söltl, M. M. C. H. van Schie, F. Hilgers, N. L. Bitzenhofer, T. Drepper, D. Rother, *Front. Catal.* **2022**, *2*, 835919.

[29] P. Gomez De Santos, S. Lazaro, J. Viña-Gonzalez, M. D. Hoang, I. Sánchez-Moreno, A. Glieder, F. Hollmann, M. Alcalde, *ACS Catal.* **2020**, *10*, 13524–13534.

[30] P. Püllmann, C. Ulpinnis, S. Marillonnet, R. Gruetzner, S. Neumann, M. J. Weissenborn, *Sci. Rep.* **2019**, *9*, 10932.

[31] C. J. Seel, A. Králík, M. Hacker, A. Frank, B. König, T. Gulder, *ChemCatChem* **2018**, *10*, 3960–3963.

[32] S. H. Lee, D. S. Choi, S. K. Kuk, C. B. Park, *Angew. Chem. Int. Ed.* **2018**, *57*, 7958–7985.

[33] J. Jeffrey Morris, E. R. Zinser, *J. Phycol.* **2013**, *49*, 1223–1228.

[34] M. Kluge, R. Ullrich, K. Scheibner, M. Hofrichter, *Green Chem.* **2012**, *14*, 440–446.

[35] S. Bierbaumer, L. Schmermund, A. List, C. K. Winkler, S. M. Glueck, W. Kroutil, *Angew. Chem. Int. Ed.* **2022**, *61*, e202117103.

[36] B. T. Nicholls, D. G. Oblinsky, S. I. Kurtoic, D. Grosheva, Y. Ye, G. D. Scholes, T. K. Hyster, *Angew. Chem. Int. Ed.* **2022**, *61*, e202113842.

[37] F. Feyza Özgen, M. E. Runda, B. O. Burek, P. Wied, J. Z. Bloh, R. Kourist, S. Schmidt, *Angew. Chem. Int. Ed.* **2020**, *59*, 3982–3987.

[38] S. Simić, M. Jakštaitė, W. T. S. Huck, C. K. Winkler, W. Kroutil, *ACS Catal.* **2022**, *12*, 14040–14049.

Angew. Chem. Int. Ed. **2023**, *62*, e202307897 (9 of 9)

© 2023 The Authors. Angewandte Chemie International Edition published by Wiley-VCH GmbH